A decision support scheme for vertebral geometry on body CT scans

Tatsuro Hayashi *[a], Huayue Chen [b], Kei Miyamoto [c], Xiangrong Zhou [a], Takeshi Hara [a], Ryujiro Yokoyama [d], Masayuki Kanematsu [d, e], Hiroaki Hoshi [f], Hiroshi Fujita [a]
[a] Department of Intelligent Image Information, Division of Regeneration and Advanced Medical Sciences, Graduate School of Medicine, Gifu University, 1-1 Yanagido, Gifu 501-1194, Japan;
[b] Department of Anatomy, Division of Disease Control, Graduate School of Medicine, Gifu University, 1-1 Yanagido, Gifu 501-1194, Japan;
[c] Department of Reconstructive Surgery for Spine, Bone, and Joint, Gifu University Graduate School of Medicine, 1-1 Yanagido, Gifu 501-1194, Japan;
[d] Radiology Services, Gifu University Graduate School of Medicine and University Hospital, 1-1 Yanagido, Gifu 501-1194, Japan;
[e] Department of Radiology, Gifu University Graduate School of Medicine and University Hospital, 1-1 Yanagido, Gifu 501-1194, Japan;
[f] Department of Radiology, Division of Tumor Control, Graduate School of Medicine, Gifu University, 1-1 Yanagido, Gifu 501-1194, Japan

ABSTRACT

For gaining a better understanding of bone quality, a great deal of attention has been paid to vertebral geometry in anatomy. The aim of this study was to design a decision support scheme for vertebral geometries. The proposed scheme consists of four parts: (1) automated extraction of bone, (2) generation of median plane image of spine, (3) detection of vertebrae, (4) quantification of vertebral body width, depth, cross-sectional area (CSA), and trabecular bone mineral density (BMD). The proposed scheme was applied to 10 CT cases and compared with manual tracking performed by an anatomy expert. Mean differences in the width, depth, CSA, and trabecular BMD were 3.1 mm, 1.4 mm, 88.7 mm^2, and 7.3 mg/cm^3, respectively. We found moderate or high correlations in vertebral geometry between our scheme and manual tracking ($r > 0.72$). In contrast, measurements obtained by using our scheme were slightly smaller than those acquired from manual tracking. However, the outputs of the proposed scheme in most CT cases were regarded to be appropriate on the basis of the subjective assessment of an anatomy expert. Therefore, if the appropriate outputs from the proposed scheme are selected in advance by an anatomy expert, the results can potentially be used for an analysis of vertebral body geometries.

Keywords: Body CT images, Vertebral body, Vertebral geometry, Vertebral width, Vertebral depth, Cross-sectional area, Bone mineral density, Computer-assisted scheme

1. INTRODUCTION

Osteoporosis has been estimated to affect more than 200 million individuals worldwide. One in three women and one in eight men are affected by osteoporosis [1]. In clinical practice, osteoporotic vertebral fracture risk is currently estimated on the basis of lumbar vertebral bone mineral density (BMD). However, vertebral fractures can occur even when the BMD does not reach the osteoporotic threshold. Previous studies have indicated that the compressive strength of vertebrae is determined not only by their bone density but also by their dimensions such as vertebral body width, height, depth, cross-sectional area (CSA), configuration, and volume [2]. In addition, reduced sagittal curvature is an independent risk factor [3]. However, the role of vertebrae in fracture risk has not been clearly demonstrated to date. Knowledge of normal vertebral anatomy is essential to understanding vertebral fracture risk.

Recently, multidetector row computed tomography (MDCT) has enabled high-resolution visualization of three-dimensional (3D) spinal structures. The MDCT method has the potential to be used for the quantitative analysis of vertebral anatomy, including BMD, geometry, and configuration, with high accuracy and precision using the same dataset. However, when thin-section CT is used to scan the whole body, a huge number of images—exceeding 1000

Medical Imaging 2011: Image Processing, edited by Benoit M. Dawant, David R. Haynor,
Proc. of SPIE Vol. 7962, 796245 · © 2011 SPIE · CCC code: 1605-7422/11/$18 · doi: 10.1117/12.877516

sections—are generated. Analysis of the spine using all these CT sections imposes a heavy burden on examiners. Therefore, it would be helpful to develop a computer-assisted scheme for analyzing vertebral dimensions on body CT images.

Several computerized schemes for the segmentation and/or identification of vertebrae had been designed to date [4–15]. Takahashi et al. [6] designed a computer-aided diagnosis (CAD) scheme for osteoporosis based on the assessment of BMD and vertebral height. However, to the best of our knowledge, no computerized scheme has been developed to date for the measurement of vertebral dimensions such as width and depth, and their relation to osteoporosis has not yet been clearly demonstrated. A population-based study of quantitative vertebral body geometry may help improve our understanding of normal vertebral anatomy, which is basic knowledge for the practice of medicine. Accordingly, the aim of this study was to design a computer-assisted scheme for the quantification of vertebral body dimensions on body thin-section CT scans. This paper proposes a computerized scheme for the measurement of vertebral body width, depth, CSA, and trabecular BMD on body CT scans.

2. METHODS

2.1 Study sample

CT images, which were obtained with a CT scanner (LightSpeed Ultra, GE Yokogawa Medical Systems Ltd., Tokyo, Japan), were scanned for the purpose of examining various organs and tissues, as is done in a metastasis check or follow-up. The scans included thoracic and lumbar vertebrae, which were scanned in each patient using standard settings (120 kV, auto mAs, 1.25-mm-thick slice, pitch = 0.63–0.74 mm). Slice intervals were modified to the same value as the pitch using sin*c* interpolation to keep each voxel in an isotropic size in 3D. The study sample consisted of 10 individuals (nine men, one woman; mean age, 55 years). Those who had a normal variant at vertebrae, as confirmed by radiologists or anatomy experts, were not included in this sample. This study was approved by the institutional review board of Gifu University.

2.2 Overview of the scheme

Measurements of vertebral body width, depth, CSA, and trabecular BMD taken by an anatomy expert are illustrated in Fig. 1. This paper presents a new computerized scheme for such measurements.

The block diagram of our proposed scheme is shown in Fig. 2. Fig. 2a shows an example of the midsagittal section of the original CT images. First, bone voxels are extracted and the center line of the spinal canal and the tips of the spinous processes are determined. Second, CT images are reformatted so that the sagittal spinal curvature disappears. The localization of vertebral bodies is done in the third step. Finally, the vertebral body contour is determined and vertebral body dimensions based on it are quantified. Each part is described below.

2.3 Bone extraction

CT numbers with bone voxels are higher than those of other internal organs. For that reason, CT number thresholding or the region-growing method is used to extract bone voxels [4]. Fig. 2b shows an example of the extraction of bone voxels. After this extraction, the center line of the spinal canal and the tips of the spinous processes are determined on the basis of implicit anatomic knowledge.

(a) Original CT images (b) Width (c) Depth (d) CSA (e) Trabecular BMD

Fig.1 Axial section view of the overlaid images between the original CT images and the manual tracking by an anatomy expert (CSA and BMD denote a cross-sectional area and bone mineral density, respectively). These are the midaxial sections of L1 and the manual tracking of vertebral body width, depth, CSA, and trabecular BMD are shown in red.

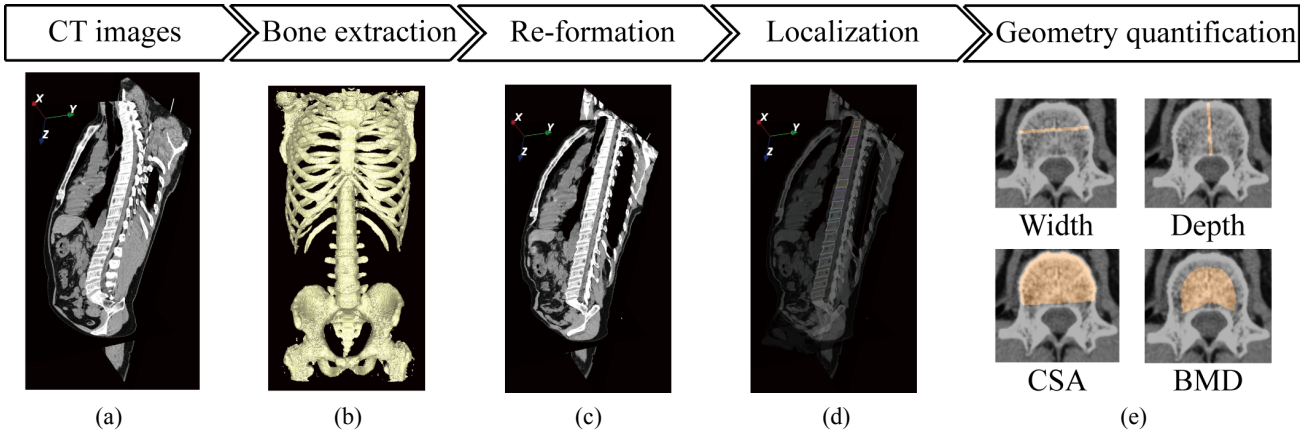

Fig.2 Block diagram of our proposed scheme. (a) The midsagittal section view of original CT images. (b) Surface view of bone voxels. (c) The midsaggital section view of re-formed CT images. (d) Section view of the overlaid images between the re-formed CT images and the points produced using the localization scheme (Localization results of individual vertebral bodies are indicated in different colors.). (e) The axial section views of the vertebral body geometries (Examples of the computerized quantification are indicated by voxels in orange.).

2.4 Image re-formation

To simplify the vertebral body detection task, CT images are reformatted. This is carried out on the basis of the center line of the spinal canal and the tips of the spinous processes [16]. Fig. 2c shows an example of the mid-sagittal section of the reformatted CT images.

2.5 Vertebral body localization

The contour model of the vertebral body is built in advance, and the vertebral body localization is carried out using the template matching technique. An example of the localization of individual vertebral bodies is indicated in Fig. 2d. Details of the localization scheme are described in [17].

2.6 Quantification of vertebral body geometry

The computerized scheme for quantifying width, depth, CSA, and trabecular BMD of vertebral bodies is described in this subsection.

Step 1: Vertebral body height (h) is identified as the distance between the uppermost and lowermost slice, including the points produced using the localization scheme, and its central section is detected as the midaxial section of the target vertebral body. The vertebral body height (h) and the midaxial section of the target vertebra are detected, and then the axial sections of $h/3$ that belong to middle sections are selected as the volume of interest (VOI) [Fig. 3(a)].

Step 2: The morphological top-hat operation is applied to the VOI. After that, a ray summation image of the VOI is generated [Fig. 3(b)] and voxels with > 20 values are extracted as contour candidates of vertebra [Fig. 3(c)].

Step 3: The vertebral contour is determined by a template matching technique with contour models of the vertebral bodies built by manual tracking of the vertebral contour on the mid-axial section [Fig. 3(d)]. In the template matching technique, rigid transformation is applied according to the following restrictions:

I. Scaling, $s\left(0.9 \le s \le 1.1\right)$, is applied to the models.

II. Rotation, $r\left(-3.0° \le r \le 3.0°\right)$, is applied to the models.

Then, the precisions of the output of Step 2 and the transformed contour models are computed, and the transformed model with the highest indicated precision is selected as the target vertebral contour. The percent of precision P of the template matching is calculated by the following equation:

$$P = \frac{P_A \cap P_B}{P_A}, \tag{1}$$

where P_A denotes voxels that make up the model and P_B denotes voxels extracted by Step 2. After that, voxels inside the vertebral contour are filled [Fig. 3(e)].

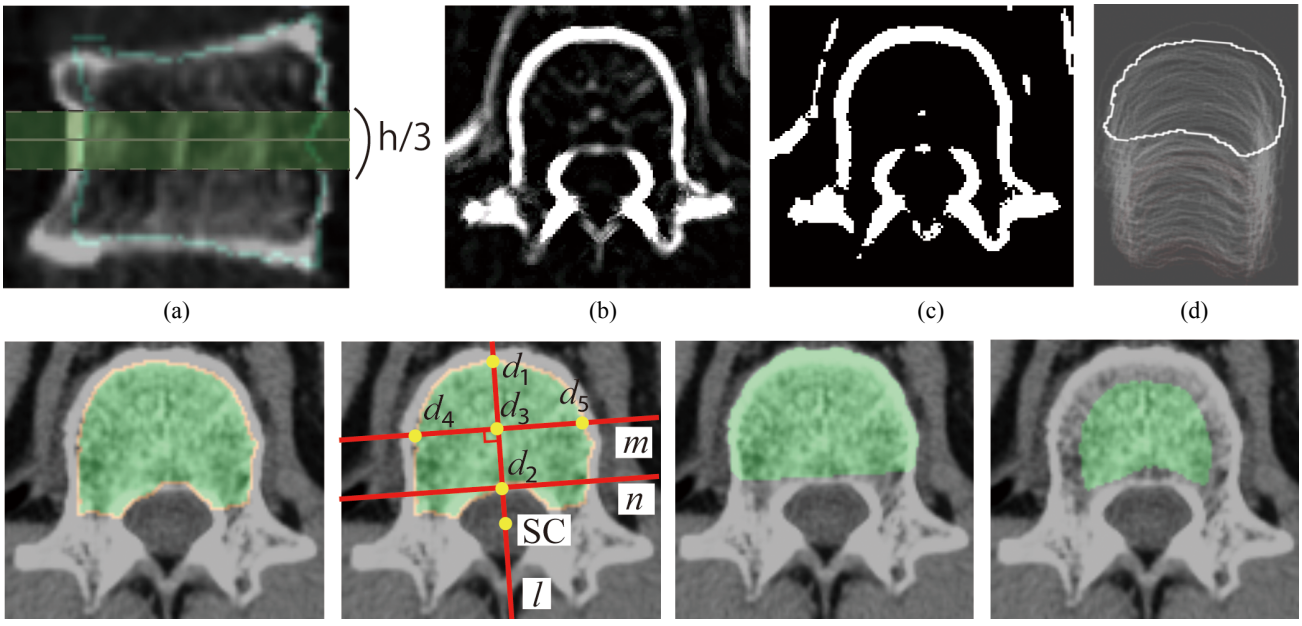

Fig.3 The proposed scheme for vertebral body geometry. (a): Volume of interest (VOI) determination on the midsagittal section (the located vertebra is shown in aqua, and the VOI is shown in green), (b): A ray summation axial view of the VOI after applying the morphological top-hat operation, (c): Binarization, (d): Contour models of the target vertebra on a midaxial section with 100 cases, (e): Model fitting on a midaxial section (the fitted contour model is shown in orange, and inside of the vertebra is shown in green), (f): Geometric definition for vertebral body geometry on a midaxial section (SC denotes the spinal canal centroid), (g): One CSA example on a midaxial section (CSA is indicated in green), (h): One BMD measurement example on the ray summation axial view of the VOI without using morphological operation (the measurement region is indicated in green).

Step 4: Line l, which divides equally the filled region that passes through the spinal canal centroid, is drawn. Next, two points, d_1 and d_2, are detected at the boundary of the line l with the filled region, and the distance between d_1 and d_2 is defined as "depth" [Fig. 2(f)].

Step 5: Line m perpendicular to line l that passes through point d_3, which is in the middle between d_1 and d_2, is drawn. Next, two points d_4 and d_5 are detected at the boundary of line m with the filled region, and the distance between d_4 and d_5 is defined as "width" [Fig. 2(f)].

Step 6: Line n parallel to line m that passes through point d_2 is drawn. Next, a cortical bone adjacent to the filled region is added as a part of the filled region. After that, the number of voxels that belongs to the filled region that is located anterior to line n is defined as "CSA" [Fig. 2(g)].

Step 7: To remove a cortical bone, voxels extracted by Step 2 are removed. After that, the morphological closing operation is applied to fill the voxels of the vertebral contour. To ensure that a cortical bone is not included, the morphological erosion operation is also applied to the extracted region.

Step 8: A ray summation image of the VOI without using the morphological operation is generated, and the mean CT number of voxels overlapping with the extracted region from Step 7 is computed. Finally, "trabecular BMD" is estimated on the basis of the mean CT number in a manner similar to [18] [Fig. 2(h)].

2.7 Assessment

The performance of our scheme is assessed by comparing it with the manual tracking done by an anatomy expert. For vertebral body width, depth, and CSA, manual tracking is carried out three times at the midaxial sections of L1 on "original" CT scans (not re-formed images), and mean values are determined to be the grand truth. Each tracking is set at a time interval of at least one week, and the position of the midaxial section of L1 is selected independently. For trabecular BMD, volumetric BMD at the central site of the vertebral body measured in [18] is used as the grand truth. Pearson's product-moment correlation coefficient (r) and Bland-Altman analysis are used to show relative and absolute reliability.

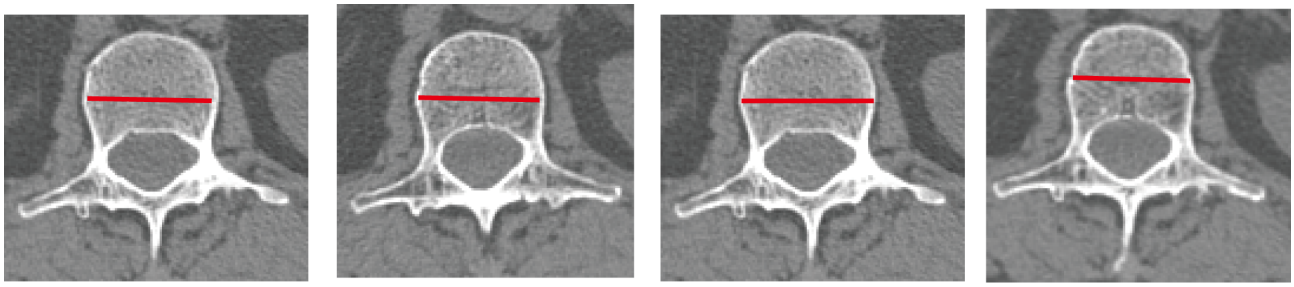

(a) width = 36.9 mm (b) width = 36.2 mm (c) width = 38.3 mm (d) width = 33.5 mm

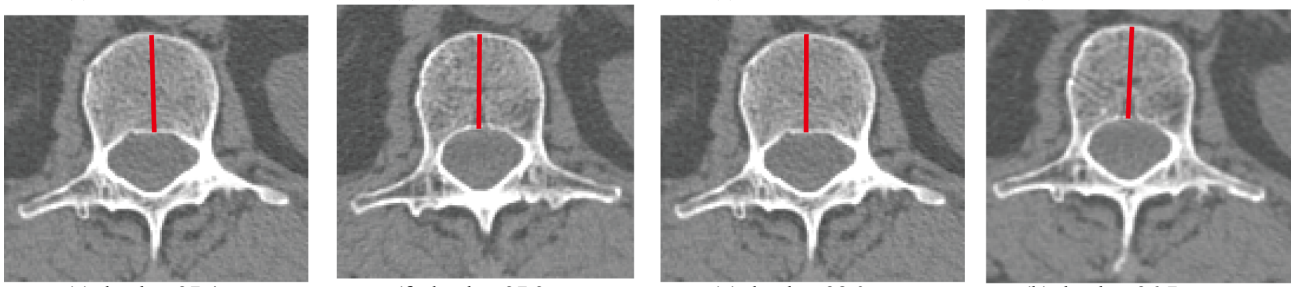

(e) depth = 27.4 mm (f) depth = 27.3 mm (g) depth = 28.0 mm (h) depth = 26.7 mm

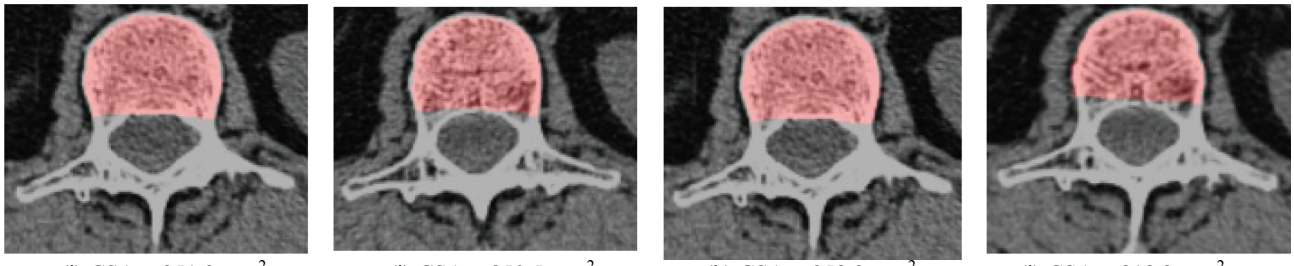

(i) CSA = 951.9 mm^2 (j) CSA = 850.5 mm^2 (k) CSA = 958.9 mm^2 (l) CSA = 818.2 mm^2

Fig.4 Measurement examples of the vertebral body width (a– d), depth (e–h), and CSA (i–l) by an anatomy expert and the proposed scheme. These are the midaxial sections of L1 and measurement results of vertebral body width, depth, and CSA are shown in red. Manual tracking of first (a, e, i), second (b, f, j), third (c, g, k) and the produced using the proposed scheme (d, h, l) are shown from left to right.

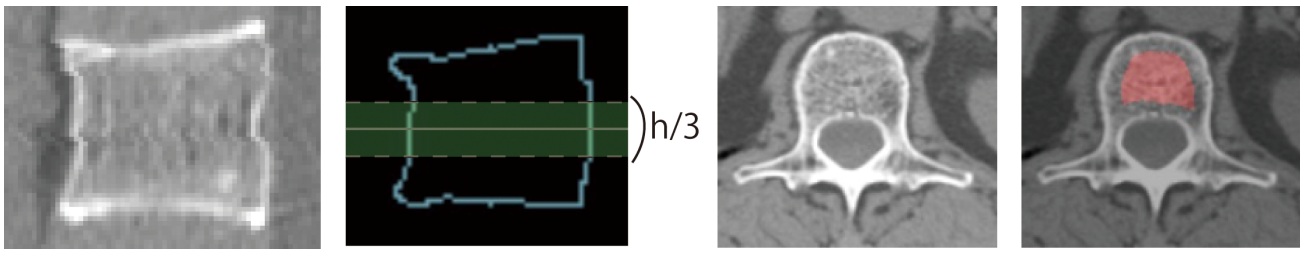

(a) (b) (c) (d) BMD = 67.8 mg/cm^3

Fig.5 Measurement example of the vertebral trabecular BMD at L1. (a): Midsagittal section on the re-formed CT images. (b) Volume of interest (VOI) determination on the midsagittal section (the located vertebra is shown in aqua, and the VOI is shown in green), (c): A ray summation axial view of VOI on the re-formed CT images, (d): BMD measurement on the ray summation axial view of the VOI (The measurement region is indicated in red).

3. RESULTS

To assess the performance of the proposed scheme, it was applied to 10 body CT cases. Vertebral contour models were built with 100 samples except for the target case. Fig. 4 illustrates the proposed scheme as well as measurement examples of vertebral body width, depth, and CSA taken by an anatomy expert. These measurements were done on the midaxial sections of L1. Fig. 4 also enables us to understand intra-observer variability and to compare manual tracking

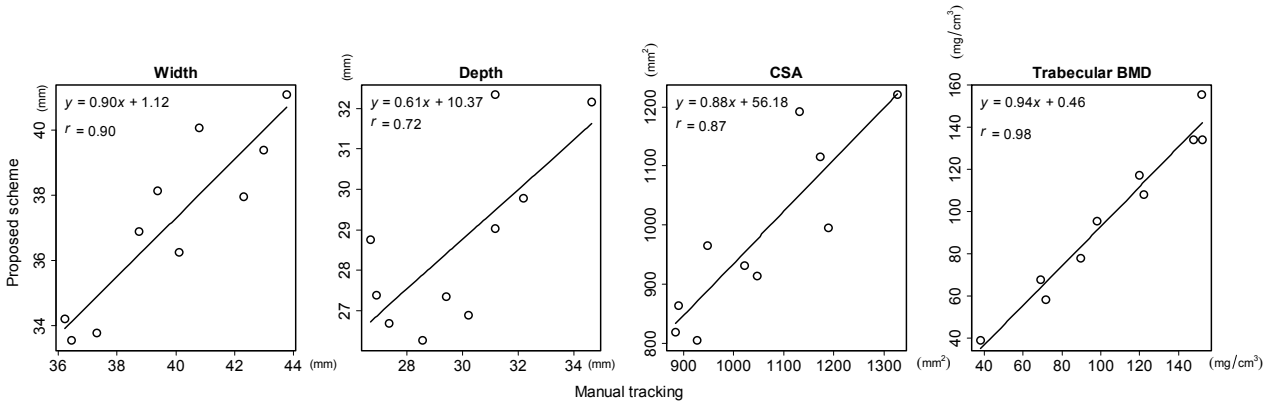

Fig.6 The correlations of vertebral geometries between the proposed scheme and manual tracking by using Pearson's product-moment correlation coefficient (Left to right: width, depth, CSA, and trabecular BMD).

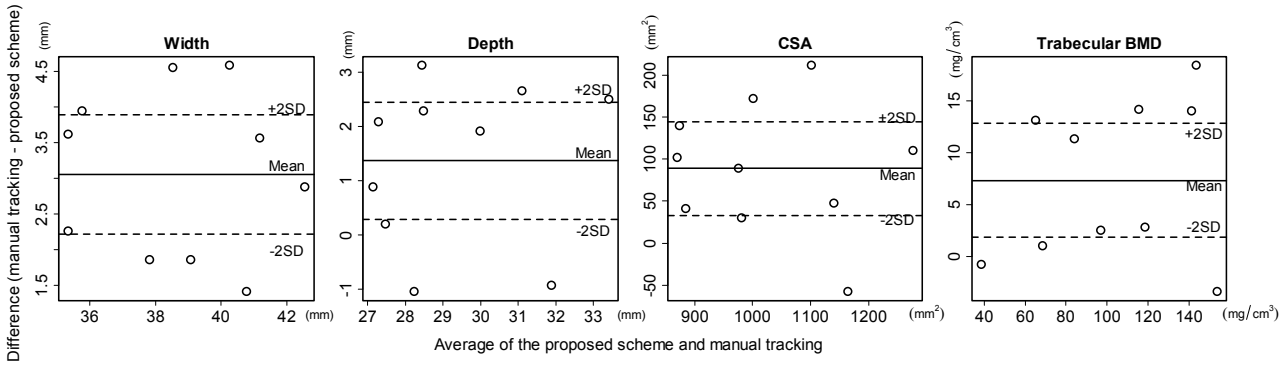

Fig.7 Bland-Altman analysis of vertebral geometries between the proposed scheme and manual tracking (Left to right: width, depth, CSA, and trabecular BMD). Three lines: mean, mean + 2 standard deviation (SD), and mean - 2 SD = limits of agreement.

with computerized tracking. Manual tracking done by an anatomy expert showed vertebral body width = 37.1 ± 1.07 mm, depth = 27.6 ± 0.38 mm, and CSA = 920.4 ± 60.7 mm^2. In contrast, computerized measurements using the proposed scheme showed vertebral body width = 33.5 mm, depth = 26.7 mm, and CSA = 818.2 mm^2. A measurement example of the vertebral trabecular BMD at L1 is illustrated in Fig. 5, which also the process flow of the proposed scheme in measuring vertebral trabecular BMD. The vertebral trabecular BMD measured by [18] was 68.9 mg/cm^3, while that measured by the proposed scheme was 67.8 mg/cm^3.

The correlations of the vertebral geometries between the proposed scheme and manual tracking are shown in Fig. 6. As can be seen, moderate correlation was found in measuring depth [r = 0.72, P = 0.02, 95% confidence interval (95% CI) of the population correlation coefficient: 0.16–0.93], and high correlations were found in measuring width (r = 0.90, P < 0.01, 95% CI: 0.63–0.98), CSA (r = 0.87, P < 0.01, 95% CI: 0.54–0.97), and trabecular BMD (r = 0.98, P < 0.01, 95% CI: 0.92–1.00), respectively.

Bland-Altman plots of vertebral geometries from the proposed scheme and the manual tracking are indicated in Fig. 7, which shows mean differences of width, depth, CSA, and trabecular BMD of 3.1 mm, 1.4 mm, 88.7 mm^2, and 7.3 mg/cm^3, respectively. No proportional biases were found for all four vertebral geometries between the proposed scheme and manual tracking when testing for no correlation. However, the 95% CI of mean associated with width, depth, CSA, and BMD did not contain zero, as seen in Fig. 7. Namely, fixed biases in measuring these vertebral geometries between two methods were found.

4. DISCUSSIONS

The aetiology of osteoporotic vertebral fractures is multifactorial, and the BMD is insufficient to evaluate correctly the risk of vertebral fracture. Several studies on vertebral geometries have been done to improve our understanding of

vertebral fracture risk [2, 3, 19–25]. For example, a systematic review of the literature that studied the potential association between vertebral fracture risk and vertebral dimensions was reported by Ruyssen-Witrand et al. [2]. Kunkel et al. [19] measured 20 vertebral parameters associated with the end plate, vertebral body, pedicle, spinal canal, spinous process, and transverse process of the human individual thoracic and lumbar vertebrae, and they created simplified geometrical models of the spine on the basis of its parameters. However, such precise measurements on medical images (especially 3D images) are a time-consuming task. For that reason, population-based studies of vertebral geometries using CT images are very challenging.

Computer-based quantitative measurements have received a lot of attention in recent years, as can be seen from examples of computer-aided volumetry (CADv) of pulmonary nodules [26]. In the area of osteoporosis analysis, Takahashi et al. [6] and Guglielmi et al. [27] have developed computer-aided schemes for evaluating the magnitude of osteoporosis on the basis of the vertebral trabecular BMD and vertebral height. Such computer-aided schemes have the potential to be used for a quantitative analysis of osteoporosis without putting a heavy burden on observers. We developed a computer-based tool for measuring thoracic and lumbar vertebral trabecular BMD using body CT scans; systematic investigation of vertebral trabecular volumetric BMD in Japanese individuals was done for the first time [18]. A novel computer-assisted scheme for evaluating sagittal spinal curvature on the basis of the center line of the spinal canal was also designed [16]. As a follow-up, in this study we attempted to design a computerized scheme for measuring vertebral body width, depth, CSA, and trabeuclar BMD.

Moderate or high correlations between the outputs of the proposed scheme and those of manual tracking were found using Pearson's product-moment correlation coefficient. However, Bland-Altman analysis showed that fixed biases were present in both methods. The thickness of a cortical bone may be one of the causes of those biases. Although the tracking by an anatomy expert was done on the basis of the center position of the cortical bone, the proposed scheme was evaluated by considering the boundary between the cortical and the trabecular bone. Adding a new procedure that converts measurement values using a regression equation may help to reduce the fixed biases.

The outputs from the proposed scheme had errors that went beyond intra-observer variability, as illustrated in Fig. 4. For that reason, it may be difficult to use the proposed scheme directly instead of with manual tracking. However, the outputs from the proposed scheme in most CT cases were regarded to be appropriate on the basis of the subjective assessment of an anatomy expert. Therefore, if the appropriate outputs from the proposed scheme are selected in advance by an anatomy expert, the results can potentially be used for analysis of vertebral body geometries. A comparison taking into account interobserver variability may be required to discuss the usefulness of the proposed scheme.

Future plans for extending this study include improving the proposed scheme so as to remove fixed biases, assessing the performance of our scheme using a large dataset, carrying out a population-based study using thin-section body CT images, and showing age-, gender-, and vertebral-level-dependent changes for vertebral body geometries.

5. CONCLUSION

A computerized scheme for measuring vertebral body width, depth, CSA, and trabecular BMD on body CT scans was designed in this study. The proposed scheme used the image re-formation technique, the vertebral body localization technique, and descriptors based on the anatomic structures of vertebrae. Experimental results for vertebral geometries showed moderate or high correlations between the proposed scheme and manual tracking. In contrast, both methods were shown to have fixed biases in measuring the vertebral geometries. However, the outputs from the proposed scheme in most CT cases were regarded to be appropriate on the basis of the subjective assessment of an anatomy expert. Therefore, if the appropriate outputs from the proposed scheme are selected in advance by an anatomy expert, its results can potentially be used for the analysis of vertebral body geometries.

ACKNOWLEDGEMENTS

The authors thank members of the Fujita Laboratory for their valuable discussions, and grateful to Gifu University Hospital staffs for preparing the CT cases, especially for Mr. T. Miyoshi and Mr. Y. Inoue. This research was supported in part by a research grant of Grant-in-Aid for Young Scientists B (21700462) from Japan Society for the Promotion of Science (JSPS), in part by a research grant from Japan Osteoporosis Foundation, and in part by a research grant of Grant-in-Aid for Scientific Research on Priority Areas (21103004) of the Ministry of Education, Culture, Sports, Science, and Technology, Japan.

REFERENCES

[1] NE Lane, "Epidemiology, etiology, and diagnosis of osteoporosis," *Am J Obstet Gynecol*, 194 (2 Suppl): S3-11 (2006)

[2] A Ruyssen-Witrand, L Gossec, S Kolta, M Dougados, and C Roux, "Vertebral dimensions as risk factor of vertebral fracture in osteoporotic patients: a systematic literature review," *Osteoporos Int*, 18 (9): 1271-8 (2007)

[3] T Kobayashi, N Takeda, Y Atsuta, T Matsuno, "Flattening of sagittal spinal curvature as a predictor of vertebral fracture," *Osteoporos Int*, 19 (1): 65-9 (2008)

[4] X Zhou, T Hayashi, M Han, H Chen, T Hara, H Fujita, R Yokoyama, M Kanematsu, and H Hoshi, "Automated segmentation and recognition of the bone structure in non-contrast torso CT images using implicit anatomical knowledge," *Proc of SPIE Medical Imaging 2009, Image Processing*, 7259: 72593S-1-72593S-4 (2009)

[5] S Furuhashi, K Abe, M Takahashi, T Aizawa, T Shizukuishi, M Sakaguchi, T Maebayashi, I Tanaka, M Narata, and Y Sasaki, "A computer-assisted system for diagnostic workstations: Automated bone labeling for CT images," *J Digit Imaging*, 22: 689-695 (2009)

[6] E Takahashi, S Saita, Y Kawata, N Niki, M Itoh, H Nishitani, and N Moriyama, "Computer aided diagnosis for osteoporosis using multi-slice CT images," *Proc of SPIE Medical Imaging 2010, Computer-Aided Diagnosis*, 7624: 76243Q-1-76243Q-8 (2010)

[7] JL Herring, BM Dawant, "Automatic lumbar vertebral identification using surface-based registration," *J Biomed Inform*, 34: 74-84 (2001)

[8] S Nishihara, H Fujita, T Iida, A Takigawa, T Hara, and X Zhou, "Evaluation of osteoporosis in X-ray CT examination: A preliminary study for an automatic recognition algorithm for the central part of a vertebral body using abdominal X-ray CT images," *Comput Med Imaging Graph*, 29: 259-266 (2005)

[9] B Naegel, "Using mathematical morphology for the anatomical labeling of vertebrae from 3D CT-scan images," *Comput Med Imaging Graph*, 31: 141-156 (2007)

[10] JJ Corso, RS Alomari, and V Chaudhary, "Lumbar disc localization and labeling with a probabilistic model on both pixel and object features," *Med Image Comput Comput Assist Interv*, 11: 202-210 (2008)

[11] S Schmidt, J Kappes, M Bergtholdt, V Pekar, S Dries, D Bystrov, and C Schnörr, "Spine detection and labeling using a parts-based graphical model," *Inf Process Med Imaging*, 20: 122-133 (2007)

[12] Y Kim, D Kim, "A fully automatic vertebra segmentation method using 3D deformable fences," *Comput Med Imaging Graph*, 33: 343-352 (2009)

[13] S Hanaoka, Y Nomura, M Nemoto, Y Masutani, E Maeda, T Yoshikawa, N Hayashi, N Yoshioka, and K Ohtomo, "Automated segmentation method for spinal column based on a dual elliptic column model and its application for virtual spinal straightening," *J Comput Assist Tomogr*, 34: 156-162 (2010)

[14] T Klinder, J Ostermann, M Ehm, A Franz, R Kneser, and C Lorenz, "Automated model-based vertebra detection, identification, and segmentation in CT images," *Med Image Anal*, 13: 471-482 (2009)

[15] J Ma, L Lu, Y Zhan, X Zhou, M Salganicoff, and A Krishnan, "Hierarchical segmentation and identification of thoracic vertebra using learning-based edge detection and coarse-to-fine deformable model," *Med Image Comput Comput Assist Interv*, 13: 19-27 (2010)

[16] T Hayashi, X Zhou, H Chen, T Hara, K Miyamoto, T Kobayashi, R Yokoyama, M Kanematsu, H Hoshi, and H Fujita, "Automated extraction method for the center line of spinal canal and its application to the spinal curvature quantification in torso X-ray CT images," *Proc. of SPIE Medical Imaging 2010, Image Processing*, 7623: 76233F-1-76233F-4 (2010)

[17] T Hayashi, H Chen, K Miyamoto, X Zhou, T Hara, R Yokoyama, M Kanematsu, H Hoshi, and H Fujita, "A computerized scheme for localization of vertebral bodies on body CT scans," *Proc. of SPIE Medical Imaging 2011, Image Processing*, in press.

[18] T Hayashi, H Chen, K Miyamoto, X Zhou, T Hara, R Yokoyama, M Kanematsu, H Hoshi, and H Fujita, "Analysis of bone mineral density distribution at trabecular bones in thoracic and lumbar vertebrae using X-ray CT images," *J Bone Miner Metab*, [Epub ahead of print].

[19] ME Kunkel, H Schmidt, and HJ Wilke, "Prediction equations for human thoracic and lumbar vertebral morphometry," *J Anat*, 216 (3): 320-8 (2010)

[20] O Sevinc, C Barut, M Is, N Eryoruk, and AA Safak, "Influence of age and sex on lumbar vertebral morphometry determined using sagittal magnetic resonance imaging," *Ann Anat*, 190 (3): 277-83 (2008)

[21] JA Junno, M Niskanen, MT Nieminen, H Maijanen, J Niinimäki, R Bloigu, and J Tuukkanen, "Temporal trends in vertebral size and shape from medieval to modern-day," *PLoS One*, 4 (3): e4836, Epub (2009)

[22] S Goh, RI Price, S Song, S Davis, and KP Singer, "Magnetic resonance-based vertebral morphometry of the thoracic spine: age, gender and level-specific influences," *Clin Biomech*, 15 (6): 417-25, (2000)
[23] D Diacinti, D Pisani, F Barone-Adesi, R Del Fiacco, S Minisola, V David, G Aliberti, and GF Mazzuoli, "A new predictive index for vertebral fractures: the sum of the anterior vertebral body heights," *Bone*, 46 (3): 768-73, (2010)
[24] S Kolta, S Quiligotti, A Ruyssen-Witrand, A Amido, D Mitton, AL Bras, W Skalli, and C Roux, "In vivo 3D reconstruction of human vertebrae with the three-dimensional X-ray absorptiometry (3D-XA) method," *Osteoporos Int*, 19 (2): 185-92, (2008)
[25] K Briot, S Kolta, J Fechtenbaum, R Said-Nahal, CL Benhamou, and C Roux, "Increase in vertebral body size in postmenopausal women with osteoporosis," *Bone*, 47 (2): 229-34, (2010)
[26] AP Reeves, AC Jirapatnakul, AM Biancardi, TV Apanasovich, C Schaefer, JJ Bowden, M Kietzmann, R Korn, M Dillmann, Q Li, J Wang, JH Moltz, JM Kuhnigk, T Hayashi, X Zhou, H Fujita, T Duindam, B van Ginneken, R Avila, JP Ko, K Melamud, H Rusinek, R Wiemker, G Soza, C Tietjen, M Thorn, MF McNitt-Gray, Y Valenciaga, M Khatonabadi, Y Kawata, and N Niki, "The VOLCANO'09 challenge: preliminary results," *Proc of the Second International Workshop on Pulmonary Image Analysis at MICCAI 2009*, 377-88, (2009)
[27] G Guglielmi, D Diacinti, C van Kuijk, F Aparisi, C Krestan, JE Adams, and TM Link, "Vertebral morphometry: current methods and recent advances," *Eur Radiol*, 18 (7): 1484-96, (2008)